

# Correlated states in super-moire materials with a kernel polynomial quantics tensor cross interpolation algorithm

Adolfo O. Fumega,<sup>1,\*</sup> Marcel Niedermeier,<sup>1,\*</sup> and Jose L. Lado<sup>1</sup>  
<sup>1</sup>*Department of Applied Physics, Aalto University, 02150 Espoo, Finland*  
 (Dated: October 4, 2024)

Super-moire materials represent a novel playground to engineer states of matter beyond the possibilities of conventional moire materials. However, from the computational point of view, understanding correlated matter in these systems requires solving models with several millions of atoms, a formidable task for state-of-the-art methods. Conventional wavefunction methods for correlated matter scale with a cubic power with the number of sites, a major challenge for super-moire materials. Here, we introduce a methodology capable of solving correlated states in super-moire materials by combining a kernel polynomial method with a quantics tensor cross interpolation algorithm based on matrix product states. This strategy leverages a mapping of the super-moire structure to a many-body Hilbert space, from which we sample with up to a hundred-fold improved efficiency due to the tensor cross interpolation backend. Individual sample evaluations are performed with a Chebyshev kernel polynomial algorithm. We demonstrate this approach with interacting super-moire systems with up to several millions of atoms, showing its ability to capture correlated states in moire-of-moire systems and domain walls between different moire systems. Our manuscript puts forward a widely applicable methodology to study correlated matter in ultra-long length scales, enabling rationalizing correlated super-moire phenomena.

## INTRODUCTION

Twisted moire materials[1] provide a unique playground to engineer artificial states of matter, including topological states[2–6], correlated phases[7–12], and superconductivity[13–17]. Moire patterns appear when two different van der Waals materials are twisted with respect to each other, leading to several coexisting length scales. Interestingly, when three or more different layers are twisted, the moire pattern itself can feature a long-range modulation, giving rise to a super-moire pattern[18–21]. Among super-moire patterns, for generic twist angles quasiperiodic patterns emerge, where recent experiments have demonstrated even more exotic states[22–24], including competing correlated mosaic orders and quasiperiodic correlated phases, as well as superconductivity[24]. From a theoretical point of view, understanding the electronic structure of moire patterns microscopically at the atomistic level requires treating interacting systems with tens of thousands of atoms[25–34], a task that pushes the limits of conventional methods[35]. Modeling super-moire patterns requires solving systems with millions of atoms and incorporating electronic interactions in a selfconsistent manner, a task challenging beyond current atomistic electronic structure methods.

The problem of dealing with very high-dimensional objects is well-known in physics, in particular in the case of quantum many-body calculations[36–38]. For a quantum many-body system with  $L$  sites, the Hilbert space has a dimension of  $2^L$ , making quantum many-body calculations extremely challenging even for moderate system sizes[39, 40]. A very successful strategy to deal with this problem is to use variational tensor network states to parametrize quantum many-body wavefunctions[36, 41–

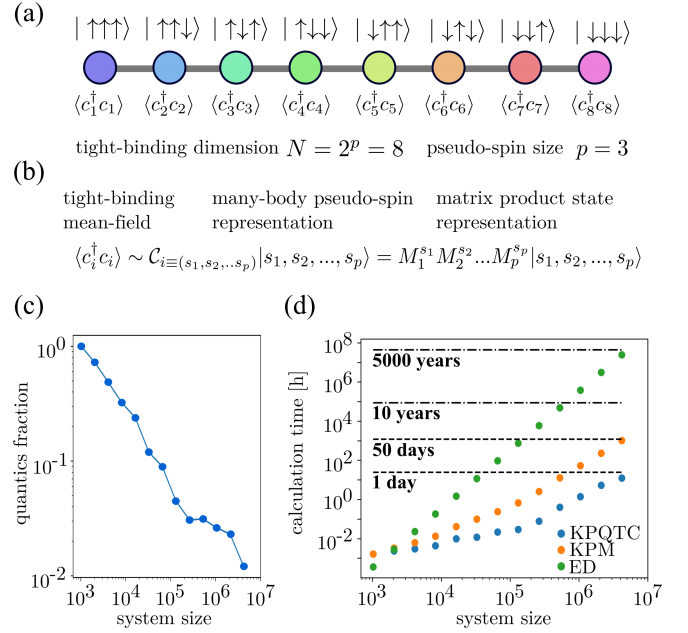


FIG. 1. (a) Schematic of the mapping between an interacting super-moire and an auxiliary many-body spin model. A many-body pseudo spin model with  $p$  spins allows us to encode the mean-field of a tight binding model with  $2^p$  sites. (b) The interacting mean-field is encoded as the amplitude of a many-body spin model as a matrix product state. Panel (c) shows the compression of the mean-field for different system sizes achieved by the algorithm. Panel (d) shows a comparison between our algorithm (KPQTC), a pure KPM method and exact diagonalization (ED).

47]. This approach allows us to solve with nearly arbitrary precision one-dimensional models, and it has provided the most accurate solutions for paradigmatic two-

dimensional models such as the doped Hubbard and frustrated Heisenberg models[48–50]. In recent years, it has been realized that the power of tensor networks parametrizing very high-dimensional objects can be applied beyond the realm of quantum many-body physics. This has led to applications in tensor networks for machine learning[51–56], quantum computing[57–64], and parsimonious function representation[65, 66]. In particular, tensor networks can be used to efficiently compress and numerically represent functions that exhibit internal structures. This suggests that this methodology may enable addressing super-moire systems, whose spatially dependent electronic structure gives rise to phenomena occurring at different length scales.

Here, we demonstrate a technique capable of solving interacting super-moire structures with several millions of atoms. Our method combines a kernel polynomial method with a quantum tensor cross interpolation (KPQTC) with matrix product states. The methodology maps the super-moire structure to a many-body Hilbert space, whose mean-field Hamiltonian is compressed in a matrix product state. This tensor network representation of the mean-field Hamiltonian is learned by applying a tensor cross-interpolation algorithm, which greatly reduces the number of real-space correlators which have to be evaluated with the (expensive) kernel polynomial method (KPM). With this methodology, we show that interacting electronic models in real space for systems with millions of atoms can be solved, allowing us to compute interaction-induced symmetry-broken states in those systems while treating interactions in a self-consistent manner. In particular, we show that this technique allows us to efficiently solve interacting super-moire models in one and two dimensions, and even in the presence of super-moire domain boundaries. Our results establish a methodology capable of dealing with interacting problems well beyond conventional wavefunction methods, providing a technique capable of addressing correlated physics in super-moire systems from microscopic models.

The paper is organized as follows. We first introduce and describe the KPQTC methodology that we have developed in this work. In the next two sections, we apply the KPQTC to the study of super-moire 1D models and 2D materials. Finally, we provide the discussion and conclusion sections highlighting the results and the broad applicability of the KPQTC method.

## METHODS

In the following, we elaborate on the methodology to solve interacting super-moire systems. We will focus on interacting fermionic models solved at the mean-field level, where the individual mean-field parameters can be computed with a kernel polynomial algorithm. The tensor cross interpolation algorithm allows us to reconstruct

the whole mean-field Hamiltonian by iteratively selecting the mean field parameters to be computed.

### Interactions in super-moire

The Hamiltonian of a super-moire system in the presence of electronic interactions takes the form

$$H = \sum_{ij} t_{ij} c_{i,s}^\dagger c_{j,s} + \sum_{ijss'} V_{ij} c_{i,s}^\dagger c_{i,s} c_{j,s'}^\dagger c_{j,s'} \quad (1)$$

where  $t_{ij}$  are the hopping parameters in the system and  $V_{ij}$  parametrizes the electronic interactions. To find the ground state of the Hamiltonian above, the interacting term can be decoupled with a mean-field ansatz of the form  $V_{ij} c_{i,s}^\dagger c_{i,s} c_{j,s'}^\dagger c_{j,s'} \approx V_{ij} \langle c_{i,s}^\dagger c_{i,s} \rangle c_{j,s'}^\dagger c_{j,s'} + \dots$  where  $\dots$  is a shorthand for the remaining Wick contractions. The previous decoupling gives rise to a mean-field Hamiltonian of the form

$$H_{MF} = \sum_{ij} t_{ij} c_{i,s}^\dagger c_{j,s} + \sum_{ijss'} \chi_{ijss'} c_{i,s}^\dagger c_{j,s'} \quad (2)$$

with  $\chi_{ijss'} \equiv \chi_{ijss'}(V_{ij}, |GS\rangle)$  the mean-field parameters, where  $|GS\rangle$  is the variational many-body ground state  $H_{MF}|GS\rangle = E_{GS}|GS\rangle$ . The variational ground state is taken as a product state of the form  $|GS\rangle = \prod_\alpha \psi_\alpha^\dagger |\Omega\rangle$ , with  $\psi_\alpha^\dagger$  variational single-particle states and  $|\Omega\rangle$  the vacuum state,  $\psi_\alpha |\Omega\rangle = 0$ . As  $H_{MF}$  depends on the  $|GS\rangle$ , and  $|GS\rangle$  depends on  $H_{MF}$ , the previous problem can be solved with a conventional iterative self-consistent algorithm. From the computational point of view, the most demanding step consists of computing the mean-field parameters  $\chi_{ijss'}$  at each step of the self-consistent procedure. In particular, for a super-moire system with  $N$  sites, conventional algorithms based on matrix diagonalization as implemented in electronic structure codes scale as  $N^3$ , whereas a full Chebyshev expansion reduces the computational cost to  $N^2$ . This sets the maximum number of sites computable with typical computational resources with diagonalization on the order of  $N = 10^4$  atoms, and with Chebyshev expansion in  $N = 10^6$  atoms. Modeling interacting states in super-moire materials requires solving problems with several millions of atoms, well above the capabilities of the previous two methods.

### Interactions with a kernel polynomial expansion

We now address how a Chebyshev kernel polynomial expansion can be used to solve self-consistent mean-field systems. In each iteration of the self-consistent procedure, the variational parameters of the mean-field Hamiltonian  $\chi_{ijss'}$  can be calculated once the correlators  $\langle c_i^\dagger c_j \rangle \equiv \langle GS | c_i^\dagger c_j | GS \rangle$  are known. These correlators can

be computed as

$$\langle c_{i,s}^\dagger c_{j,s'} \rangle = \int_{-\infty}^{\epsilon_F} \langle \Omega | c_{j,s'} \delta(\omega - \mathcal{H}_{\text{MF}}) c_{i,s}^\dagger | \Omega \rangle d\omega \quad (3)$$

where  $\epsilon_F$  is the single particle Fermi energy and  $\delta(\omega - \mathcal{H}_{\text{MF}})$  is the Dirac-delta function operator. Taking  $\langle c_{i,s}^\dagger c_{j,s'} \rangle = \int_{-\infty}^{\epsilon_F} g_{ijss'}(\omega) d\omega$  with  $g_{ijss'}(\omega) = \langle \Omega | c_{j,s'} \delta(\omega - \mathcal{H}_{\text{MF}}) c_{i,s}^\dagger | \Omega \rangle$ , where  $g_{ijss'}(\omega)$  is the dynamical correlator between sites  $i$  and  $j$  with spin  $s$  and  $s'$ . For the sake of concreteness, we now take that the Hamiltonian  $\mathcal{H}_{\text{MF}}$  has a single particle spectrum bounded in the interval  $(-1, 1)$ . The function  $g_{ijss'}(\omega)$  can be efficiently computed with a Chebyshev kernel polynomial expansion[67] of the form  $g_{ijss'}(\omega) = \frac{1}{\pi\sqrt{1-\omega^2}} [\gamma_0 T_0(\omega) + 2 \sum_{n>0} \gamma_n T_n(\omega)]$ , where  $T_n(\omega)$  are the Chebyshev polynomials and  $\gamma_n$  are the coefficients of the expansion. Thanks to the Chebyshev recursion relation, the moments of the expansion can be computed as  $\gamma_n = \langle \Omega | c_{j,s'} | v_n \rangle$ , where  $|v_{n+1}\rangle = 2\mathcal{H}_{\text{MF}}|v_n\rangle - |v_{n-1}\rangle$ , with  $|v_1\rangle = \mathcal{H}_{\text{MF}}|v_0\rangle$  and  $|v_0\rangle = c_{i,s}^\dagger | \Omega \rangle$ . The calculation of a single correlator  $\langle c_i^\dagger c_j \rangle$  scales linearly with the number of atoms  $N$ . To compute the self-consistent Hamiltonian, the number of correlators that have to be evaluated is proportional to the number of atoms  $N$ , so that a Chebyshev kernel polynomial expansion allows us to perform self-consistent calculations[68] with a scaling  $N^2$ , in contrast the scaling  $N^3$  for exact diagonalization.

### Quantics tensor-network representation of the mean-field Hamiltonian

The most expensive part of the algorithm is to evaluate the variational parameters  $\chi_{ijss'}$  of the mean-field Hamiltonian. The  $\chi_{ijss'}$ 's depend on the correlators  $\langle c_i^\dagger c_j \rangle = \langle GS | c_i^\dagger c_j | GS \rangle$ , and where each  $\langle c_i^\dagger c_j \rangle$  has to be found by performing a full run of the KPM algorithm. Therefore, to perform the full mean-field calculation, a large number of KPM's has to be executed. In the following, we will apply the tensor cross interpolation algorithm to construct an approximation of the function  $\chi_{ijss'}(\{\langle c_i^\dagger c_j \rangle\})$  as a matrix product state:

$$\chi_{ijss'} \approx M_1^{s_1} M_2^{s_2} \dots M_p^{s_p}. \quad (4)$$

The main benefit of this method is, that it allows us to construct a high-fidelity approximation of  $\chi_{ijss'}$ , while only requiring an exact evaluation for a very small number of arguments  $\langle c_i^\dagger c_j \rangle$ . All other correlators, that are not called during the construction of  $\chi_{ij}$ , do not need to be calculated in the first place, which greatly reduces the number of individual KPM runs, the most expensive part of the algorithm. A schematic of the mapping used by the KPQTC is shown in Fig. 1.

The kernel polynomial tensor cross interpolation method relies on exploiting the natural structure and

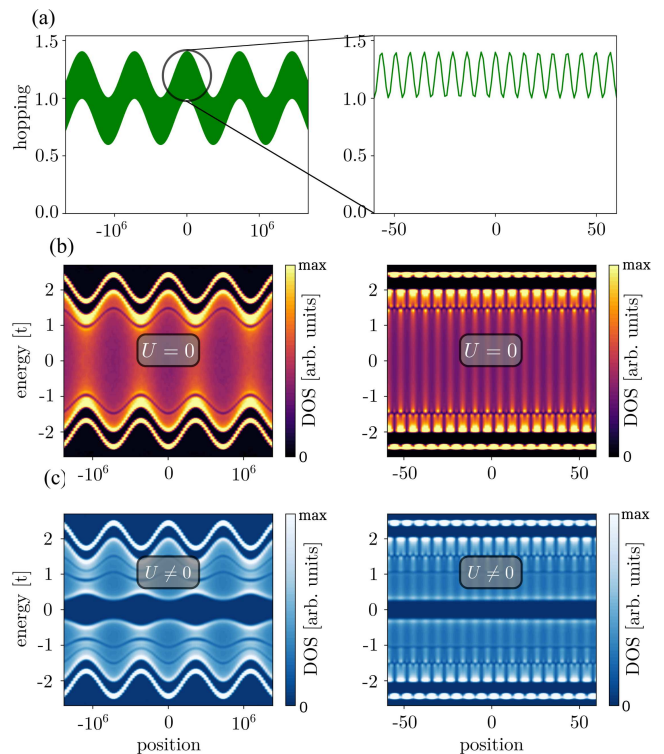


FIG. 2. **Correlated super-moire for  $L = 2^{22}$  sites** (above 4 million sites). Panel (a) shows the super-moire modulation of the Hamiltonian, featuring a moire pattern at short scales, and another at long length scales. Panel (b) shows the density of states in the system at long and short length scales, showing how its spectral properties are modulated. Panel (c) shows the spectral function of the interacting super-lattice solved self-consistently with KPQTC. It is observed that the interaction-induced gap in the spectral function is modulated in the long length scale, whereas its intensity is modulated at the short length scale.

length scales of the mean-field Hamiltonian in a super-moire system. The large number of components of  $\chi_{ijss'}(\{\langle c_i^\dagger c_j \rangle\})$  can be reformulated as a rank- $R$  tensor  $\chi^{\sigma_1 \dots \sigma_R}$ , with  $R \propto \log(\text{number of correlators})$ . This tensor can be re-expressed as a much cheaper matrix product state, using the tensor cross interpolation algorithm, which learns a quasi-optimal approximation of  $\chi^{\sigma_1 \dots \sigma_R}$  by evaluating it exactly for only a small subset of its entries[65, 69–74]. Therefore, only a small subset of the full list  $[\langle c_1^\dagger c_1 \rangle, \dots, \langle c_{2^p}^\dagger c_{2^p} \rangle]$  of real-space correlators has to be calculated in practice. Furthermore, the architecture of the underlying matrix product state and the update strategy is dynamically optimized during the self-consistent loop, where at each iteration we optimize for the strategy that requires the least amount of evaluations of the mean-field of the previous iteration. The dynamically optimized parameters include the matrix product state bond dimension, the number of orbitals for which independent matrix product states are created, the initial

pivot, the choice of a rook or accumulative optimization method, and the number and location of global pivots.

## INTERACTIONS IN SUPER-MOIRE 1D MODELS

We now use the KPQTC method to address one-dimensional models. First, we will focus on a system that features two incommensurate moire patterns, also incommensurate with the lattice. Second, we will address a system featuring an interface between two moire patterns, to show that the methodology is able to deal with inhomogeneous problems. While 1D models are not the most relevant use case for van der Waals materials, they provide an excellent testing ground for the KPQTC algorithm to show that calculations with millions of atoms can be performed.

### Incommensurate 1D super-moire

We first consider a model featuring two moire patterns, incommensurate with each other and with the original lattice. Super-moire models can be realized in artificial platforms including engineering optical resonators and cold atom systems[75, 76]. Furthermore, within van der Waals materials, the electronic properties of multiwalled nanotubes are effectively described by a one-dimensional super-moire Hamiltonian[77]. We take a Hamiltonian of the form

$$\mathcal{H} = \sum_{ij,s} t_{ij} c_{i,s}^\dagger c_{j,s} + U \sum_i \left[ c_{i,\uparrow}^\dagger c_{i,\uparrow} - \frac{1}{2} \right] \left[ c_{i,\downarrow}^\dagger c_{i,\downarrow} - \frac{1}{2} \right], \quad (5)$$

where the hopping is modulated by two incommensurate moire patterns as

$$t_{n,n+1} = t_0 + t_1 \cos(k_1 X_{n,n+1}) + t_2 \cos(k_2 X_{n,n+1}), \quad (6)$$

with  $X_{n,n+1} = (x_n + x_{n+1})/2$ ,  $k_1$  and  $k_2$  the wavevectors of the two moires and  $x_n$  is the location of site  $n$ . We take  $k_1 = 2\pi/5\sqrt{2}$  and  $k_2 = 2\pi/5/2^{p-1}\sqrt{3}$ , which leads to two incommensurate modulations, also incommensurate with the lattice. The modulation in the local hopping gives rise to a different competition between electronic interactions and kinetic energy in different regions in the system. We solve the model with the QTCI for a system with  $L = 2^{22}$  sites, approximately 4 million atoms. The results of our calculation are shown in Fig. 2, where we show the moire modulation of the Hamiltonian at the two length scales, together with the non-interacting (Fig. 2b) and interacting (Fig. 2c) local spectral function. In particular, we observe that interactions give rise to a spatially dependent gap opening, as shown by comparing the density of states in the absence (Fig. 2b) and presence (Fig. 2c) of electronic interactions. Interestingly,

on the largest length scale, the gap opening fully follows the moire length scale, whereas, on the shorter length scale, the spectrum shows a modulation of the spectral weight. This stems from the fact that at the smaller moire length scale, the correlation length associated with the electronic order is of the same order as the moire length scale, which gives rise to the lowest electronic excitation to extend in the whole moire. In contrast, for the biggest moire length scale, the correlation length associated with the order is much smaller than the length scale of the moire, which leads to the spectral gap being modulated exactly following the moire.

The performance of the KPQTC method[78, 79] as compared to the current techniques is highlighted in Fig. 1. Figure 1c shows the compression of the mean-field components introduced by the KPQTC. The fraction of real-space correlators required as compared to the pure KPM is plotted as a function of the system size. We can clearly observe the advantage introduced by the KPQTC method for large systems above  $10^5$  sites, where the fraction of correlators required decreases as the system size grows. The convergence time of the self-consistent mean-field calculation for the KPQTC method is reported in Fig. 1d. We show the estimated calculation times for the pure KPM and the ED methods are shown for comparison. We can observe that our KPQTC allows solving systems of millions of atoms in less than one day, while the traditional KPM requires around 50 days. KPM and KPQTC become faster than exact diagonalization once the system size goes above  $10^3$  sites, and KPQTC becomes substantially faster than KPM for systems above  $10^5$  sites. Therefore, these results demonstrate the advantage of the KPQTC method to study correlated states in super-moire materials composed of millions of atoms.

### Super-moire domain wall in 1D

An alternative situation that appears in super-moire systems is a domain wall between different length scales. This emerges in situations where structural relaxations strongly prefer specific stacking or moire length scales, a phenomenon that gives rise to domain walls appearing between different regions. We will here consider a system where the shortest moire length scale is the same in the whole system, whereas the biggest one features two domains. We take the hopping  $t_{n,n+1}$  to be modulated in space by two wavelengths  $k_1$  and  $\bar{k}_2$ , one of them spatially dependent

$$t_{n,n+1} = t_0 + t_1 \cos(k_1 X_{n,n+1}) + t_2 \cos(\bar{k}_2(X_{n,n+1})X_{n,n+1}), \quad (7)$$

with the wavelength of the modulation featuring a domain wall:

$$\bar{k}_2(X_{n,n+1}) = \bar{k}_2(1 + \delta \tanh(X_{n,n+1}/W)). \quad (8)$$



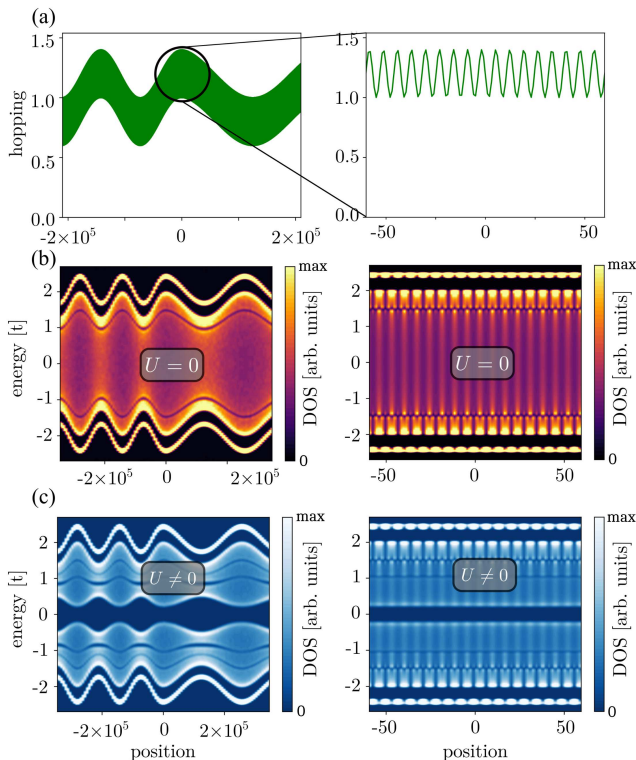


FIG. 3. **Correlated super-moire domain wall for  $L = 2^{20}$  sites** (above 1 million sites). Panel (a) shows the super-moire modulation featuring a domain wall, featuring different super-moire modulations at the left and right boundary. Panel (b) shows the density of states in the system at long and short length scales, showing how its spectral properties are modulated according to each domain. Panel (c) shows the spectral function of the interacting system solved selfconsistently with KPQTC. The interaction-induced gap in the spectral function is modulated in the long length scale following the super-moire at each domain, whereas at the domain wall its intensity is modulated following the local moire.

Here,  $W$  describes the width of the domain wall and  $\delta$  parametrizes the mismatch between the length scales of the moire modulations in the two domains, that in the asymptotic limit are  $k_2(1 - \delta)$  and  $k_2(1 + \delta)$ . In our calculations, we have used  $\delta = 0.2$ ,  $W = 2^p/40$ ,  $k_2 = 2\pi 5/2^{p-1}\sqrt{3}$  and  $k_1 = 2\pi/5\sqrt{2}$ . This Hamiltonian therefore describes a system breaking translational symmetry regardless of the moire length. In Fig. 3, we show the solution of the interacting model for  $2^{21}$  sites, or approximately 2 million atoms. The impact of the electronic interactions can be observed by comparing the non-interacting (Fig. 3b) and interacting (Fig. 3c) spectral functions. The gap in the spectral function follows the moire pattern both in the left and right domains at the longest length scale. As in the case studied previously, this phenomenology stems from the fact that both moire length scales are much longer than the localization length associated with the correlated state, which leads

to a spectral gap reflecting the large-scale moire modulation. At shorter scales, the spectrum is modulated according to the moire, but leading to a spectral gap that is uniform due to the comparable correlation and moire length scales.

## INTERACTIONS IN SUPER-MOIRE 2D MATERIALS

We now consider interacting super-moire materials in two dimensions, which is the most physically relevant scenario for van der Waals materials. We will focus on the Hamiltonian of a purely two-dimensional system of super-moire graphene monolayer. Moire patterns in monolayer graphene can emerge from periodically modulated strain from buckling[80–84], or from a moire pattern with boron nitride. For the sake of concreteness, we will focus on the case of periodically buckled monolayer graphene, which has been demonstrated to lead to a variety of correlated states. The Hamiltonian of the system thus takes the form

$$\mathcal{H} = \sum_{\langle ij \rangle, s} t_{ij} c_{i,s}^\dagger c_{j,s} + U \sum_i \left[ c_{i,\uparrow}^\dagger c_{i,\uparrow} - \frac{1}{2} \right] \left[ c_{i,\downarrow}^\dagger c_{i,\downarrow} - \frac{1}{2} \right], \quad (9)$$

where the sites  $ij$  form a honeycomb lattice and  $\langle ij \rangle$  runs over the first neighbors in the graphene honeycomb lattice. In the presence of buckling, the hopping parameters  $t_{ij}$  of graphene are modified as[81, 83, 84]

$$t_{ij} = t_{ij}^0 (1 + \delta \sin(\Omega \mathbf{u}_{ij} \cdot \mathbf{R}_{ij})), \quad (10)$$

where  $\mathbf{R}_{ij} = (\mathbf{r}_i + \mathbf{r}_j)/2$  is the location of the bond,  $\mathbf{u}_{ij}$  is the vector linking sites  $i$  and  $j$ , and  $\Omega$  parametrizes the frequency of the buckling. The previous modulation gives rise to a direction-dependent modulation of the hopping of wavevector  $\Omega$ . The previous buckling modulation gives rise to pseudo-Landau levels due to the emergence of a non-uniform artificial gauge field. The pseudo-Landau levels get localized in an emergent honeycomb lattice structure due to the modulation of the gauge field. In the presence of interactions, those localized modes give rise to a correlated state.

We will study two cases where super-moire physics emerges in this system. First, we will consider the case where two different bucklings at different length scales emerge, with relative frequencies  $\Omega_M$  and  $\Omega_{SM}$  and strengths  $\delta_M$  and  $\delta_{SM}$ . Afterwards, we will consider an interface between two buckling modulations.

### Correlations in a 2D super-moire

We start first with the moire of moire buckling. In this scenario, the hoppings of the graphene monolayer

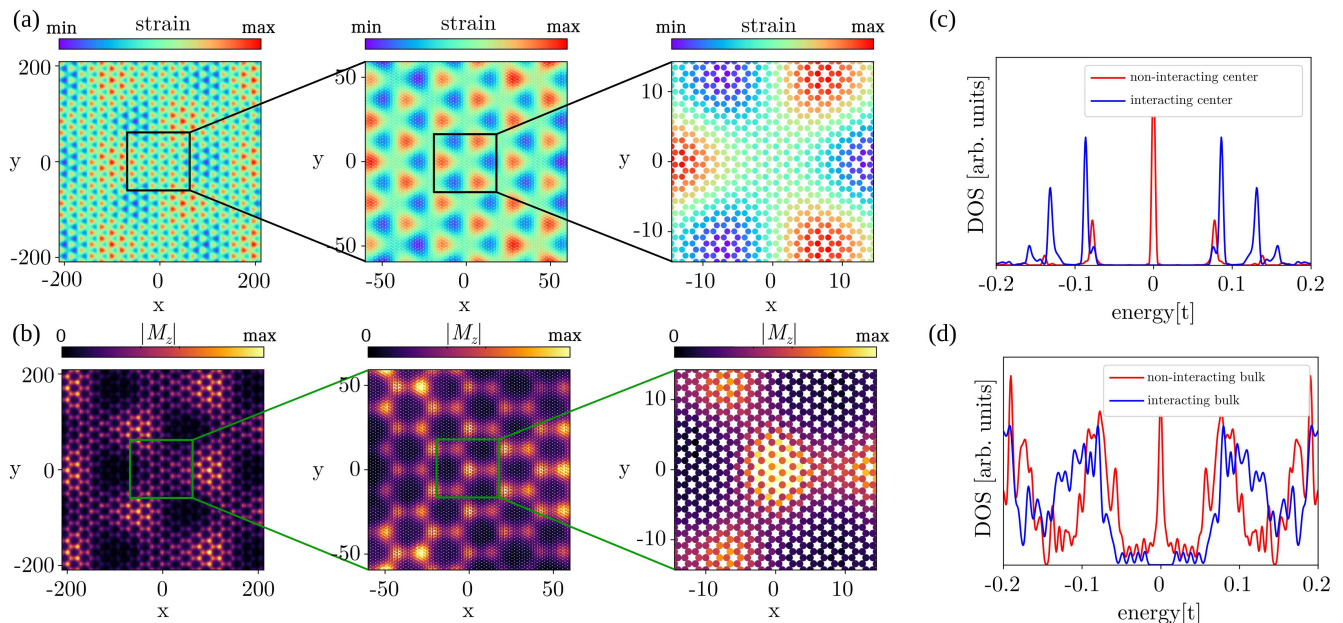


FIG. 4. **2D super-moire:** Panel (a) shows the profile of strain in the super-moire system, showing a modulation of the strain both at a large length scale and at a shorter one. Panel (b) shows the self-consistent magnetization computed with KPQTC algorithm. We observe that the order parameter is modulated both at the super-moire and moire length scales, giving rise to localized regions of space with electronic order. Panels (c,d) show the spectral function in the absence and presence of electronic interactions, both at the center of the super-moire pattern (c) and averaged over the super-moire pattern (d). We observe that interactions give rise to a gap in the spectral function, associated with a correlated insulating state in the buckled super-moire. Self-consistent calculations are performed in systems with more than 200000 sites ( $N = 2^{18}$ ).

are modulated as

$$t_{ij} = t_{ij}^0 (1 + \delta_M \sin(\Omega_M \mathbf{u}_{ij} \cdot \mathbf{R}_{ij})) (1 + \delta_{SM} \sin(\Omega_{SM} \mathbf{u}_{ij} \cdot \mathbf{R}_{ij})), \quad (11)$$

where  $\delta_M$  and  $\delta_{SM}$  correspond to the strength of the buckling at the moire and super-moire length scales, and  $\Omega_M$ ,  $\Omega_{SM}$  are the wavevectors of the moire and super-moire buckling. In Fig. 4a, we show the strength of the local strain field at each point in space, defined as the average value of the neighboring hopping  $s(\mathbf{r}_i) \sim \sum_j t_{ij}$ . We solve a system with  $2^{18}$ , or approximately 200000, sites, where the self-consistent magnetization is shown in Fig. 4b. We observe that the symmetry broken order clearly follows both moire patterns, giving rise to an emergent honeycomb lattice modulated at the super-moire length scale of magnetic order. We can now compare the spectral function of the system both with and without interactions, as shown in Fig. 4cd. In particular, in Fig. 4c we show the local spectral function right at the center of the super-moire pattern. In the absence of interactions, a zero energy peak emerges, in the presence of interactions gives rise to a gap (Fig. 4c). Such zero energy mode is precisely the one responsible for the spatially localized magnetic order as shown in the shortest length scale of Fig. 4b. Figure 4d shows the comparison of the spectral function computed in the whole

length scale of the super-moire pattern. We observe that in the absence of correlations, the system features a gapless electron gas with a van Hove singularity at charge neutrality, whereas in the presence of interactions a full band gap opens up (Fig. 4d). Such a van Hove singularity corresponds to the localized modes in specific regions of the moire pattern, which in the interacting regime give rise to a correlated insulator in the full system.

### Correlations between moire domains

In the presence of two moire patterns stemming from several twisted two-dimensional materials, structural relaxations can lead to relatively uniform moire regions separated from each other by domain walls[21, 85–87]. This phenomenology observed experimentally requires that computational methods be capable of dealing with geometries lacking translational symmetry and hosting a very large amount of atoms. We now show that the KPQTC methodology is able to capture correlated states emerging in the presence of moire domains. For the sake of concreteness, we will focus on studying a domain wall between two different bucklings in graphene. In this scenario, the hopping of the graphene system will be modulated as

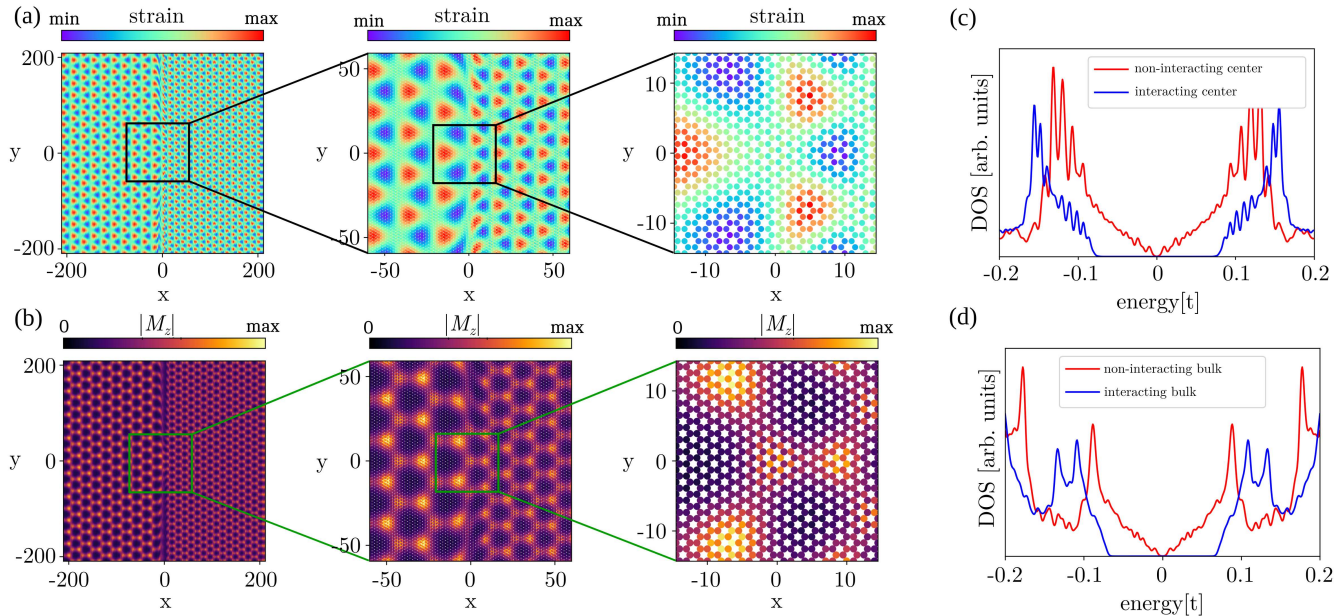


FIG. 5. **2D moire domain wall:** Panel (a) shows the profile of strain in a domain wall in the moire system, featuring a different moire on the left and on the right. Panel (b) shows the self-consistent magnetization computed with KPQTC algorithm. The order parameter follows the moire at the two domains, while also featuring a modulation at the domain wall. Panels (c,d) show the spectral function in the absence and presence of electronic interactions, both at the center of the domain wall (c), and averaged over a length scale around the domain wall on the order of the super-moire length scale (d). Interactions give rise to a gap in the spectral function at the domain wall, that coexists with the correlated state in the two domains. Self-consistent calculations are performed in systems with more than 200000 sites ( $N = 2^{18}$ ).

$$t_{ij} = t_{ij}^0 (1 + \delta \sin(\Omega(\mathbf{R}_{ij}) \mathbf{u}_{ij} \cdot \mathbf{R}_{ij})), \quad (12)$$

where now the buckling wavevector changes in space and features a domain wall of the form

$$\Omega(\mathbf{R}_{ij}) = \bar{\Omega}(1 + \delta \tanh(X_{ij}/W)). \quad (13)$$

Here  $W$  parametrizes the width of the moire domain wall and  $\delta$  controls the difference between the two moire buckling frequencies, which asymptotically inside the domain become  $\bar{\Omega}(1 - \delta)$  and  $\bar{\Omega}(1 + \delta)$ .

The spatial modulation of the strain is shown in Fig. 5(a) at different length scales. At the right and left domains the strain profile corresponds to a buckled monolayer, yet featuring different modulation length scales. When introducing electronic interactions (Fig. 5b), a moire correlated state emerges, featuring an order parameter following the modulation of the strain in the left and right domains. Interestingly, certain regions develop a correlated order at the interface between the two domains, whereas in other regions of the domain wall, the correlated order is quenched (Fig. 5b). This phenomenology is due to the mismatch in the non-uniform strain between the two domains in different regions of the domain wall. With the correlated state, the spectral

function of the system can be computed both at the center of the domain wall (Fig. 5c), or averaged over a large length scale (Fig. 5d). In the absence of interactions, the system remains gapless, featuring a linear dispersion close to the domain wall (Fig. 5c). In the presence of interactions, the whole system develops a correlated insulating state, including the domain wall, thus giving rise to a full spectral gap in the system (Fig. 5d).

## DISCUSSION

We have shown that the kernel polynomial tensor cross algorithm enables us to solve interacting super-moire models with several millions of atoms. While our calculations focus on Hubbard models, our methodology can be used to compress and infer a generic mean-field Hamiltonian, including in the presence of non-local interactions. In particular, beyond the magnetic orders we have considered in our manuscript, it is worth noting that a similar strategy can be used to capture charge order, superconducting or valley coherent states[10], which are especially relevant for twisted graphene multilayers. The energy resolution of our algorithm is set by the number of Chebyshev polynomials. Symmetry-broken states with very small energy scales, such as superconducting order, require a higher number of Chebyshev polynomials. A



key step is that the models we considered have a certain structure, both in the single-particle Hamiltonian and its mean-field. The tensor cross interpolation algorithm relies on the existence of a compressibility in the mean-field Hamiltonian.

While this is true for generic twisted van der Waals materials, even in the presence of domain walls, systems with strong disorder may represent a challenge for our algorithm. This stems from the fact that in the presence of strong disorder, the compressibility of the mean-field is lost due to randomness, thus substantially increasing the required number of evaluations to reconstruct the mean-field. This is however not a limitation in the presence of a finite dilute amount of impurities, and thus the KPQTC methodology would allow us to tackle super-moire systems with a small amount of impurities. It is important to note that the choice of pivots and update strategy of tensors can strongly influence the required number of evaluations required to converge the tensor network. As work in quantum tensor cross interpolation methods is progressing rapidly, we foresee that further improvements in these algorithms will enable us to address more complex and bigger interacting super-moire systems.

In our manuscript, we have used a matrix product state representation of the mean-field terms, yet the Hamiltonian is still stored as a sparse matrix. With this algorithm, the maximum system size is determined by the required kernel polynomial expansion with vector for  $N$  sites, which requires storing vectors of size  $N$ , where memory becomes the bottleneck. A potential step in the future is to store the Hamiltonian itself as a matrix product operator, such that the kernel polynomial expansion is done directly with tensor networks. This would allow us to reach system sizes beyond  $N = 10^8$ . It is also worth noting that since the evaluations of each individual correlator with the kernel polynomial algorithm are fully independent, our approach can be massively parallelized to thousands of cores almost with linear scaling[88]. This should be contrasted with electronic structure methods based on diagonalization, where diagonalization tasks show a worse than linear scaling with parallelization. While our calculations have focused on correlated states in tight binding models, a similar approach to the one presented here can be implemented in conventional Hartree-Fock quantum chemistry codes and density functional theory, in particular, those based on describing the electronic density and Hamiltonian on real space grids[89–93].

## CONCLUSION

Solving interacting models in super-moire materials represents a formidable theory challenge to understanding emerging phenomena in van der Waals materials, due

to the unprecedented system sizes required to capture their physics. Here, we have presented a kernel polynomial tensor cross interpolation algorithm, that can solve interacting models with several millions of atoms, considerably outperforming the current state-of-the-art. Our strategy relies on mapping the mean-field Hamiltonian of a large electronic model to an auxiliary many-body Hilbert space that is compressed using a many-body tensor network. The tensor network is constructed with a tensor cross interpolation algorithm, which greatly reduces the number of individual evaluations performed with a kernel polynomial method. This demonstrates how a quantum-inspired methodology enables massive speed-up of the calculation of mean-field interacting ground states of tight-binding models. We have applied our algorithm to both one- and two-dimensional models, showing that this approach allows us to deal with interacting problems with multiple long-range modulations and domain walls. In particular, we have demonstrated that this methodology can describe correlated states in super-moire buckled graphene, capturing both the electronic reconstructions and symmetry-breaking at the moire and super-moire length scales. Our methodology enables tackling the interacting models with a number of sites required to rationalize the physics of a whole new family of artificial materials based on twisted van der Waals heterostructures. In particular, it can be readily extended to account for charge order, bond-ordered, topological and superconducting states, providing the required computational tool to study super-moire quantum matter.

**Acknowledgements:** We acknowledge financial support from the Academy of Finland Projects Nos. 331342, 358088, and 349696, InstituteQ, the Jane and Aatos Erkko Foundation, and the Finnish Quantum Flagship. We thank X. Waintal, C. Groth, A. Moulinas, N. Jolly, T. Louvet, M. Srdinsek, A. Manesco, O. Zilberberg, B. Amorim, E. Castro, P. San-Jose and C. Flindt for useful discussions. We acknowledge the computational resources provided by the Aalto Science-IT project.

---

\* These authors contributed equally.

- [1] E. Y. Andrei, D. K. Efetov, P. Jarillo-Herrero, A. H. MacDonald, K. F. Mak, T. Senthil, E. Tutuc, A. Yazdani, and A. F. Young, The marvels of moiré materials, *Nature Reviews Materials* **6**, 201–206 (2021).
- [2] Y. Zeng, Z. Xia, K. Kang, J. Zhu, P. Knüppel, C. Vaswani, K. Watanabe, T. Taniguchi, K. F. Mak, and J. Shan, Thermodynamic evidence of fractional chern insulator in moiré mote2, *Nature* **622**, 69–73 (2023).
- [3] M. Serlin, C. L. Tschirhart, H. Polshyn, Y. Zhang, J. Zhu, K. Watanabe, T. Taniguchi, L. Balents, and A. F. Young, Intrinsic quantized anomalous hall effect in a moiré heterostructure, *Science* **367**, 900–903 (2020).
- [4] A. L. Sharpe, E. J. Fox, A. W. Barnard, J. Finney,



- K. Watanabe, T. Taniguchi, M. A. Kastner, and D. Goldhaber-Gordon, Emergent ferromagnetism near three-quarters filling in twisted bilayer graphene, *Science* **365**, 605–608 (2019).
- [5] P. Rickhaus, J. Wallbank, S. Slizovskiy, R. Pisoni, H. Overweg, Y. Lee, M. Eich, M.-H. Liu, K. Watanabe, T. Taniguchi, T. Ihn, and K. Ensslin, Transport through a network of topological channels in twisted bilayer graphene, *Nano Letters* **18**, 6725–6730 (2018).
- [6] J. Cai, E. Anderson, C. Wang, X. Zhang, X. Liu, W. Holtzmann, Y. Zhang, F. Fan, T. Taniguchi, K. Watanabe, Y. Ran, T. Cao, L. Fu, D. Xiao, W. Yao, and X. Xu, Signatures of fractional quantum anomalous hall states in twisted mote2, *Nature* **622**, 63–68 (2023).
- [7] Y. Cao, V. Fatemi, A. Demir, S. Fang, S. L. Tomarken, J. Y. Luo, J. D. Sanchez-Yamagishi, K. Watanabe, T. Taniguchi, E. Kaxiras, R. C. Ashoori, and P. Jarillo-Herrero, Correlated insulator behaviour at half-filling in magic-angle graphene superlattices, *Nature* **556**, 80–84 (2018).
- [8] G. W. Burg, E. Khalaf, Y. Wang, K. Watanabe, T. Taniguchi, and E. Tutuc, Emergence of correlations in alternating twist quadrilayer graphene, *Nature Materials* **21**, 884–889 (2022).
- [9] A. Kerelsky, L. J. McGilly, D. M. Kennes, L. Xian, M. Yankowitz, S. Chen, K. Watanabe, T. Taniguchi, J. Hone, C. Dean, A. Rubio, and A. N. Pasupathy, Maximized electron interactions at the magic angle in twisted bilayer graphene, *Nature* **572**, 95–100 (2019).
- [10] H. Kim, Y. Choi, E. Lantagne-Hurtubise, C. Lewandowski, A. Thomson, L. Kong, H. Zhou, E. Baum, Y. Zhang, L. Holleis, K. Watanabe, T. Taniguchi, A. F. Young, J. Alicea, and S. Nadj-Perge, Imaging inter-valley coherent order in magic-angle twisted trilayer graphene, *Nature* **623**, 942–948 (2023).
- [11] X. Lu, P. Stepanov, W. Yang, M. Xie, M. A. Aamir, I. Das, C. Urgell, K. Watanabe, T. Taniguchi, G. Zhang, A. Bachtold, A. H. MacDonald, and D. K. Efetov, Superconductors, orbital magnets and correlated states in magic-angle bilayer graphene, *Nature* **574**, 653–657 (2019).
- [12] W. Zhao, B. Shen, Z. Tao, Z. Han, K. Kang, K. Watanabe, T. Taniguchi, K. F. Mak, and J. Shan, Gate-tunable heavy fermions in a moiré kondo lattice, *Nature* **616**, 61–65 (2023).
- [13] Y. Cao, V. Fatemi, S. Fang, K. Watanabe, T. Taniguchi, E. Kaxiras, and P. Jarillo-Herrero, Unconventional superconductivity in magic-angle graphene superlattices, *Nature* **556**, 43 (2018).
- [14] M. Yankowitz, S. Chen, H. Polshyn, Y. Zhang, K. Watanabe, T. Taniguchi, D. Graf, A. F. Young, and C. R. Dean, Tuning superconductivity in twisted bilayer graphene, *Science* **363**, 1059–1064 (2019).
- [15] J. M. Park, Y. Cao, K. Watanabe, T. Taniguchi, and P. Jarillo-Herrero, Tunable strongly coupled superconductivity in magic-angle twisted trilayer graphene, *Nature* **590**, 249–255 (2021).
- [16] M. Oh, K. P. Nuckolls, D. Wong, R. L. Lee, X. Liu, K. Watanabe, T. Taniguchi, and A. Yazdani, Evidence for unconventional superconductivity in twisted bilayer graphene, *Nature* **600**, 240–245 (2021).
- [17] J. M. Park, Y. Cao, L.-Q. Xia, S. Sun, K. Watanabe, T. Taniguchi, and P. Jarillo-Herrero, Robust superconductivity in magic-angle multilayer graphene family, *Nature Materials* **21**, 877–883 (2022).
- [18] T. Devakul, P. J. Ledwith, L.-Q. Xia, A. Uri, S. C. de la Barrera, P. Jarillo-Herrero, and L. Fu, Magic-angle helical trilayer graphene, *Science Advances* **9**, 10.1126/sciadv.adi6063 (2023).
- [19] M. Kapfer, B. S. Jessen, M. E. Eisele, M. Fu, D. R. Danielsen, T. P. Darlington, S. L. Moore, N. R. Finney, A. Marchese, V. Hsieh, P. Majchrzak, Z. Jiang, D. Biswas, P. Dudin, J. Avila, K. Watanabe, T. Taniguchi, S. Ulstrup, P. Bøggild, P. J. Schuck, D. N. Basov, J. Hone, and C. R. Dean, Programming twist angle and strain profiles in 2d materials, *Science* **381**, 677–681 (2023).
- [20] Y. Li, M. Xue, H. Fan, C.-F. Gao, Y. Shi, Y. Liu, K. Watanabe, T. Taniguchi, Y. Zhao, F. Wu, X. Wang, Y. Shi, W. Guo, Z. Zhang, Z. Fei, and J. Li, Symmetry breaking and anomalous conductivity in a double-moiré superlattice, *Nano Letters* **22**, 6215–6222 (2022).
- [21] S. Turkel, J. Swann, Z. Zhu, M. Christos, K. Watanabe, T. Taniguchi, S. Sachdev, M. S. Scheurer, E. Kaxiras, C. R. Dean, and A. N. Pasupathy, Orderly disorder in magic-angle twisted trilayer graphene, *Science* **376**, 193–199 (2022).
- [22] Y. Li, F. Zhang, V.-A. Ha, Y.-C. Lin, C. Dong, Q. Gao, Z. Liu, X. Liu, S. H. Ryu, H. Kim, C. Jozwiak, A. Bostwick, K. Watanabe, T. Taniguchi, B. Kousa, X. Li, E. Rotenberg, E. Khalaf, J. A. Robinson, F. Giustino, and C.-K. Shih, Tuning commensurability in twisted van der waals bilayers, *Nature* **625**, 494–499 (2024).
- [23] S. J. Ahn, P. Moon, T.-H. Kim, H.-W. Kim, H.-C. Shin, E. H. Kim, H. W. Cha, S.-J. Kahng, P. Kim, M. Koshino, Y.-W. Son, C.-W. Yang, and J. R. Ahn, Dirac electrons in a dodecagonal graphene quasicrystal, *Science* **361**, 782–786 (2018).
- [24] A. Uri, S. C. de la Barrera, M. T. Randeria, D. Rodan-Legrain, T. Devakul, P. J. D. Crowley, N. Paul, K. Watanabe, T. Taniguchi, R. Lifshitz, L. Fu, R. C. Ashoori, and P. Jarillo-Herrero, Superconductivity and strong interactions in a tunable moiré quasicrystal, *Nature* **620**, 762–767 (2023).
- [25] E. Suárez Morell, J. D. Correa, P. Vargas, M. Pacheco, and Z. Barticevic, Flat bands in slightly twisted bilayer graphene: Tight-binding calculations, *Phys. Rev. B* **82**, 121407 (2010).
- [26] L. A. Gonzalez-Arraga, J. L. Lado, F. Guinea, and P. San-Jose, Electrically controllable magnetism in twisted bilayer graphene, *Phys. Rev. Lett.* **119**, 107201 (2017).
- [27] M. Long, P. A. Pantaleón, Z. Zhan, F. Guinea, J. A. Silva-Guillén, and S. Yuan, An atomistic approach for the structural and electronic properties of twisted bilayer graphene-boron nitride heterostructures, *npj Computational Materials* **8**, 10.1038/s41524-022-00763-1 (2022).
- [28] A. Julku, T. J. Peltonen, L. Liang, T. T. Heikkilä, and P. Törmä, Superfluid weight and berezinskii-kosterlitz-thouless transition temperature of twisted bilayer graphene, *Phys. Rev. B* **101**, 060505 (2020).
- [29] A. O. Sboychakov, A. L. Rakhmanov, A. V. Rozhkov, and F. Nori, Electronic spectrum of twisted bilayer graphene, *Phys. Rev. B* **92**, 075402 (2015).
- [30] A. Ramires and J. L. Lado, Emulating heavy fermions in twisted trilayer graphene, *Phys. Rev. Lett.* **127**, 026401 (2021).
- [31] L. Baldo, T. Löthman, P. Holmval, and A. M. Black-

- Schaffer, Defect-induced band restructuring and length scales in twisted bilayer graphene, *Phys. Rev. B* **108**, 125141 (2023).
- [32] M. S. Ramzan, Z. A. H. Goodwin, A. A. Mostofi, A. Kuc, and J. Lischner, Effect of coulomb impurities on the electronic structure of magic angle twisted bilayer graphene, *npj 2D Materials and Applications* **7**, 10.1038/s41699-023-00403-2 (2023).
- [33] A. Ramires and J. L. Lado, Electrically tunable gauge fields in tiny-angle twisted bilayer graphene, *Phys. Rev. Lett.* **121**, 146801 (2018).
- [34] Y. Mao, D. Guerci, and C. Mora, Supermoiré low-energy effective theory of twisted trilayer graphene, *Phys. Rev. B* **107**, 125423 (2023).
- [35] S. Carr, S. Fang, and E. Kaxiras, Electronic-structure methods for twisted moiré layers, *Nature Reviews Materials* **5**, 748–763 (2020).
- [36] R. Orús, A practical introduction to tensor networks: Matrix product states and projected entangled pair states, *Annals of Physics* **349**, 117–158 (2014).
- [37] G. Carleo and M. Troyer, Solving the quantum many-body problem with artificial neural networks, *Science* **355**, 602–606 (2017).
- [38] M. Cerezo, A. Arrasmith, R. Babbush, S. C. Benjamin, S. Endo, K. Fujii, J. R. McClean, K. Mitarai, X. Yuan, L. Cincio, and P. J. Coles, Variational quantum algorithms, *Nature Reviews Physics* **3**, 625–644 (2021).
- [39] D. P. Arovas, E. Berg, S. A. Kivelson, and S. Raghu, The hubbard model, *Annual Review of Condensed Matter Physics* **13**, 239–274 (2022).
- [40] M. Qin, T. Schäfer, S. Andergassen, P. Corboz, and E. Gull, The hubbard model: A computational perspective, *Annual Review of Condensed Matter Physics* **13**, 275–302 (2022).
- [41] S. R. White, Density matrix formulation for quantum renormalization groups, *Phys. Rev. Lett.* **69**, 2863 (1992).
- [42] R. Orús, Tensor networks for complex quantum systems, *Nature Reviews Physics* **1**, 538–550 (2019).
- [43] U. Schollwöck, The density-matrix renormalization group in the age of matrix product states, *Annals of Physics* **326**, 96–192 (2011).
- [44] J. Haegeman, C. Lubich, I. Oseledets, B. Vandereycken, and F. Verstraete, Unifying time evolution and optimization with matrix product states, *Phys. Rev. B* **94**, 165116 (2016).
- [45] U. Schollwöck, The density-matrix renormalization group, *Rev. Mod. Phys.* **77**, 259 (2005).
- [46] J. I. Cirac, D. Pérez-García, N. Schuch, and F. Verstraete, Matrix product states and projected entangled pair states: Concepts, symmetries, theorems, *Rev. Mod. Phys.* **93**, 045003 (2021).
- [47] M. Fishman, S. R. White, and E. M. Stoudenmire, The ITensor Software Library for Tensor Network Calculations, *SciPost Phys. Codebases* , 4 (2022).
- [48] B.-X. Zheng, C.-M. Chung, P. Corboz, G. Ehlers, M.-P. Qin, R. M. Noack, H. Shi, S. R. White, S. Zhang, and G. K.-L. Chan, Stripe order in the underdoped region of the two-dimensional hubbard model, *Science* **358**, 1155–1160 (2017).
- [49] S. Marten, G. Bollmark, T. Köhler, S. R. Manmana, and A. Kantian, Transient superconductivity in three-dimensional Hubbard systems by combining matrix-product states and self-consistent mean-field theory, *SciPost Phys.* **15**, 236 (2023).
- [50] G. Bollmark, T. Köhler, L. Pizzino, Y. Yang, J. S. Hofmann, H. Shi, S. Zhang, T. Giamarchi, and A. Kantian, Solving 2d and 3d lattice models of correlated fermions—combining matrix product states with mean-field theory, *Phys. Rev. X* **13**, 011039 (2023).
- [51] E. Stoudenmire and D. J. Schwab, Supervised learning with tensor networks, in *Advances in Neural Information Processing Systems*, Vol. 29, edited by D. Lee, M. Sugiyama, U. Luxburg, I. Guyon, and R. Garnett (Curran Associates, Inc., 2016).
- [52] E. M. Stoudenmire, Learning relevant features of data with multi-scale tensor networks, *Quantum Science and Technology* **3**, 034003 (2018).
- [53] R. Dilip, Y.-J. Liu, A. Smith, and F. Pollmann, Data compression for quantum machine learning, *Phys. Rev. Res.* **4**, 043007 (2022).
- [54] Z.-Y. Han, J. Wang, H. Fan, L. Wang, and P. Zhang, Unsupervised generative modeling using matrix product states, *Phys. Rev. X* **8**, 031012 (2018).
- [55] T.-D. Bradley, E. M. Stoudenmire, and J. Terilla, Modeling sequences with quantum states: a look under the hood, *Machine Learning: Science and Technology* **1**, 035008 (2020).
- [56] S. Cheng, L. Wang, T. Xiang, and P. Zhang, Tree tensor networks for generative modeling, *Phys. Rev. B* **99**, 155131 (2019).
- [57] Y. Zhou, E. M. Stoudenmire, and X. Waintal, What limits the simulation of quantum computers?, *Phys. Rev. X* **10**, 041038 (2020).
- [58] J. Tindall, M. Fishman, E. M. Stoudenmire, and D. Sels, Efficient tensor network simulation of ibm’s eagle kicked ising experiment, *PRX Quantum* **5**, 010308 (2024).
- [59] M. Niedermeier, M. Nairn, C. Flindt, and J. L. Lado, Quantum computing topological invariants of two-dimensional quantum matter, *arXiv e-prints* , arXiv:2404.06048 (2024), arXiv:2404.06048 [quant-ph].
- [60] F. Pan, K. Chen, and P. Zhang, Solving the sampling problem of the sycamore quantum circuits, *Phys. Rev. Lett.* **129**, 090502 (2022).
- [61] F. Pan and P. Zhang, Simulation of quantum circuits using the big-batch tensor network method, *Phys. Rev. Lett.* **128**, 030501 (2022).
- [62] M. Niedermeier, J. L. Lado, and C. Flindt, Simulating the quantum fourier transform, grover’s algorithm, and the quantum counting algorithm with limited entanglement using tensor networks, *Phys. Rev. Res.* **6**, 033325 (2024).
- [63] S.-X. Zhang, J. Allcock, Z.-Q. Wan, S. Liu, J. Sun, H. Yu, X.-H. Yang, J. Qiu, Z. Ye, Y.-Q. Chen, C.-K. Lee, Y.-C. Zheng, S.-K. Jian, H. Yao, C.-Y. Hsieh, and S. Zhang, Tensorcircuit: a quantum software framework for the nisq era, *Quantum* **7**, 912 (2023).
- [64] G. Torlai and M. Fishman, *PastaQ: A package for simulation, tomography and analysis of quantum computers* (2020).
- [65] M. K. Ritter, Y. Núñez Fernández, M. Wallerberger, J. von Delft, H. Shinaoka, and X. Waintal, Quantics tensor cross interpolation for high-resolution parsimonious representations of multivariate functions, *Phys. Rev. Lett.* **132**, 056501 (2024).
- [66] K. Sakaue, H. Shinaoka, and R. Sakurai, Learning tensor trains from noisy functions with application to quantum simulation, *arXiv e-prints* , arXiv:2405.12730 (2024), arXiv:2405.12730 [quant-ph].
- [67] A. Weiße, G. Wellein, A. Alvermann, and H. Fehske,

- The kernel polynomial method, *Rev. Mod. Phys.* **78**, 275 (2006).
- [68] Y. Nagai, Y. Ota, and M. Machida, Efficient numerical self-consistent mean-field approach for fermionic many-body systems by polynomial expansion on spectral density, *Journal of the Physical Society of Japan* **81**, 024710 (2012).
- [69] Y. Núñez Fernández, M. Jeannin, P. T. Dumitrescu, T. Kloss, J. Kaye, O. Parcollet, and X. Waintal, Learning feynman diagrams with tensor trains, *Phys. Rev. X* **12**, 041018 (2022).
- [70] Y. Núñez Fernández, M. K. Ritter, M. Jeannin, J.-W. Li, T. Kloss, T. Louvet, S. Terasaki, O. Parcollet, J. von Delft, H. Shinaoka, and X. Waintal, Learning tensor networks with tensor cross interpolation: new algorithms and libraries, *arXiv e-prints*, [arXiv:2407.02454](https://arxiv.org/abs/2407.02454) (2024), [arXiv:2407.02454](https://arxiv.org/abs/2407.02454) [physics.comp-ph].
- [71] A. Erpenbeck, W.-T. Lin, T. Blommel, L. Zhang, S. Iskakov, L. Bernheimer, Y. Núñez Fernández, G. Cohen, O. Parcollet, X. Waintal, and E. Gull, Tensor train continuous time solver for quantum impurity models, *Phys. Rev. B* **107**, 245135 (2023).
- [72] M. Jeannin, Y. Núñez Fernández, T. Kloss, O. Parcollet, and X. Waintal, Cross-extrapolation reconstruction of low-rank functions and application to quantum many-body observables in the strong coupling regime, *Phys. Rev. B* **110**, 035124 (2024).
- [73] N. Jolly, Y. Núñez Fernández, and X. Waintal, Tensorized orbitals for computational chemistry, *arXiv e-prints*, [arXiv:2308.03508](https://arxiv.org/abs/2308.03508) (2023), [arXiv:2308.03508](https://arxiv.org/abs/2308.03508) [cond-mat.str-el].
- [74] M. Murray, H. Shinaoka, and P. Werner, Nonequilibrium diagrammatic many-body simulations with quantum tensor trains, *Phys. Rev. B* **109**, 165135 (2024).
- [75] P. Wang, Y. Zheng, X. Chen, C. Huang, Y. V. Kartashov, L. Torner, V. V. Konotop, and F. Ye, Localization and delocalization of light in photonic moiré lattices, *Nature* **577**, 42–46 (2019).
- [76] Q. Fu, P. Wang, C. Huang, Y. V. Kartashov, L. Torner, V. V. Konotop, and F. Ye, Optical soliton formation controlled by angle twisting in photonic moiré lattices, *Nature Photonics* **14**, 663–668 (2020).
- [77] I. Caha, L. Boddapatti, A. u. Ahmad, M. Banobre, A. T. Costa, A. N. Enyashin, W. Li, P. Gargiani, M. Valvidares, J. Fernandez-Rossier, and F. L. Deepak, Magnetic single wall CrI3 nanotubes encapsulated within multiwall Carbon Nanotubes, *arXiv e-prints*, [arXiv:2405.14967](https://arxiv.org/abs/2405.14967) (2024), [arXiv:2405.14967](https://arxiv.org/abs/2405.14967) [cond-mat.mtrl-sci].
- [78] pyqula library, <https://github.com/joselado/pyqula>.
- [79] qtcipy library, <https://github.com/joselado/qtcipy>.
- [80] J. Mao, S. P. Milovanović, M. Andelković, X. Lai, Y. Cao, K. Watanabe, T. Taniguchi, L. Covaci, F. M. Peeters, A. K. Geim, Y. Jiang, and E. Y. Andrei, Evidence of flat bands and correlated states in buckled graphene superlattices, *Nature* **584**, 215–220 (2020).
- [81] A. L. R. Manesco and J. L. Lado, Correlation-induced valley topology in buckled graphene superlattices, *2D Materials* **8**, 035057 (2021).
- [82] Q. Gao, J. Dong, P. Ledwith, D. Parker, and E. Khalaf, Untwisting moire physics: Almost ideal bands and fractional chern insulators in periodically strained monolayer graphene, *Phys. Rev. Lett.* **131**, 096401 (2023).
- [83] X. Wan, S. Sarker, S.-Z. Lin, and K. Sun, Topological exact flat bands in two-dimensional materials under periodic strain, *Phys. Rev. Lett.* **130**, 216401 (2023).
- [84] V. T. Phong and E. J. Mele, Boundary modes from periodic magnetic and pseudomagnetic fields in graphene, *Phys. Rev. Lett.* **128**, 176406 (2022).
- [85] N. Nakatsuji, T. Kawakami, and M. Koshino, Multiscale lattice relaxation in general twisted trilayer graphenes, *Phys. Rev. X* **13**, 041007 (2023).
- [86] I. M. Craig, M. Van Winkle, C. Groschner, K. Zhang, N. Dowlatshahi, Z. Zhu, T. Taniguchi, K. Watanabe, S. M. Griffin, and D. K. Bediako, Local atomic stacking and symmetry in twisted graphene trilayers, *Nature Materials* **23**, 323–330 (2024).
- [87] R. Engelke, H. Yoo, S. Carr, K. Xu, P. Cazeaux, R. Allen, A. M. Valdivia, M. Luskin, E. Kaxiras, M. Kim, J. H. Han, and P. Kim, Topological nature of dislocation networks in two-dimensional moiré materials, *Phys. Rev. B* **107**, 125413 (2023).
- [88] M. Kreutzer, A. Pieper, G. Hager, G. Wellein, A. Alvermann, and H. Fehske, Performance engineering of the kernel polynomial method on large-scale cpu-gpu systems, in *2015 IEEE International Parallel and Distributed Processing Symposium*, Vol. 78 (IEEE, 2015) p. 417–426.
- [89] L. Kronik, A. Makmal, M. L. Tiago, M. M. G. Alemany, M. Jain, X. Huang, Y. Saad, and J. R. Chelikowsky, Parsec – the pseudopotential algorithm for real-space electronic structure calculations: recent advances and novel applications to nano-structures, *physica status solidi (b)* **243**, 1063–1079 (2006).
- [90] J. C. A. Prentice, J. Aarons, J. C. Womack, A. E. A. Allen, L. Andrinopoulos, L. Anton, R. A. Bell, A. Bhandari, G. A. Bramley, R. J. Charlton, R. J. Clements, D. J. Cole, G. Constantinescu, F. Corsetti, S. M.-M. Dubois, K. K. B. Duff, J. M. Escartín, A. Greco, Q. Hill, L. P. Lee, E. Linscott, D. D. O’Regan, M. J. S. Phipps, L. E. Ratcliff, A. R. Serrano, E. W. Tait, G. Teobaldi, V. Vitale, N. Yeung, T. J. Zuehlsdorff, J. Dziejcz, P. D. Haynes, N. D. M. Hine, A. A. Mostofi, M. C. Payne, and C.-K. Skylaris, The onetep linear-scaling density functional theory program, *The Journal of Chemical Physics* **152**, 10.1063/5.0004445 (2020).
- [91] A. V. Ivanov, G. Levi, E. O. Jónsson, and H. Jónsson, Method for calculating excited electronic states using density functionals and direct orbital optimization with real space grid or plane-wave basis set, *Journal of Chemical Theory and Computation* **17**, 5034–5049 (2021).
- [92] J. J. Mortensen, A. H. Larsen, M. Kuisma, A. V. Ivanov, A. Taghizadeh, A. Peterson, A. Haldar, A. O. Dohn, C. Schäfer, E. O. Jónsson, E. D. Hermes, F. A. Nilsson, G. Kastlunger, G. Levi, H. Jónsson, H. Häkkinen, J. Fojt, J. Kangsabanik, J. Sødequist, J. Lehtomäki, J. Heske, J. Enkovaara, K. T. Winther, M. Dulak, M. M. Melander, M. Ovesen, M. Louhivuori, M. Walter, M. Gjerding, O. Lopez-Acevedo, P. Erhart, R. Warmbier, R. Würdemann, S. Kaappa, S. Latini, T. M. Boland, T. Bligaard, T. Skovhus, T. Susi, T. Maxson, T. Rossi, X. Chen, Y. L. A. Schmerwitz, J. Schiøtz, T. Olsen, K. W. Jacobsen, and K. S. Thygesen, Gpaw: An open python package for electronic structure calculations, *The Journal of Chemical Physics* **160**, 10.1063/5.0182685 (2024).
- [93] J. M. Soler, E. Artacho, J. D. Gale, A. García, J. Junquera, P. Ordejón, and D. Sánchez-Portal, The siesta method for ab initio order-n materials simulation, *Journal of Physics: Condensed Matter* **14**, 2745–2779 (2002).